Internal Structure of InP/ZnS Nanocrystals Unraveled by High-Resolution Soft X-ray Photoelectron Spectroscopy

Kai Huang,[†] Renaud Demadrille,[†] Mathieu G. Silly,[‡] Fausto Sirotti,[‡] Peter Reiss,[†,*] and Olivier Renault[§,*]

[†]CEA Grenoble, INAC/SPrAM (UMR 5819 CEA-CNRS-UJF)/LEMOH, 17 rue des Martyrs, 38054 Grenoble Cedex 9, France, [‡]Synchrotron SOLEIL, L'Orme des Merisiers, Saint-Aubin, BP 48, 91192 Gif sur Yvette Cedex, France, and [§]CEA, LETI, MINATEC, 38054 Grenoble Cedex 9, France

ABSTRACT High-energy resolution photoelectron spectroscopy ($\Delta E < 200$ meV) is used to investigate the internal structure of semiconductor quantum dots containing low *Z*-contrast elements. In InP/ZnS core/shell nanocrystals synthesized using a single-step procedure (core and shell precursors added at the same time), a homogeneously alloyed InPZnS core structure is evidenced by quantitative analysis of their In3$d_{5/2}$ spectra recorded at variable excitation energy. When using a two-step method (core InP nanocrystal synthesis followed by subsequent ZnS shell growth), XPS analysis reveals a graded core/shell interface. We demonstrate the existence of In—S and S_x—In—P_{1-x} bonding states in both types of InP/ZnS nanocrystals, which allows a refined view on the underlying reaction mechanisms.

KEYWORDS: nanocrystals · X-ray photoelectron spectroscopy · indium phosphide · core/shell structure · alloys

Semiconductor nanocrystals (NCs), also named quantum dots (QDs), are intensely studied due to their unique optical and electronic properties. Of particular interest for both basic and applied research are the size-dependent fluorescence properties of various II—VI (*e.g.*, CdSe, CdTe), III—V (InP, InAs), IV—VI (PbSe, PbS), and I—III—VI ($CuInS_2$, $CuInSe_2$) semiconductor NCs. After initial studies in the 1990s, indium phosphide QDs have regained attention as an alternative to Cd-based NCs during the past few years due to the development of novel chemical synthesis routes which allow producing high-quality samples in short reaction times.

As for most other types of QDs, also for InP, the surface passivation with a larger band gap semiconductor yielding a core/shell structure is used to improve their fluorescence quantum yield (QY) and photostability.[1] ZnS with a bulk band gap of 3.6 eV is generally applied as the shell material for InP NCs, despite its relatively large lattice mismatch in the cubic zinc blende phase (7.6%).[2−7] Core/shell InP/ZnS NCs are usually prepared in a two-step (TS) procedure at high temperature: (i) synthesis of the InP core NCs, (ii) overcoating with the ZnS shell. The QY of InP/ZnS NCs synthesized by the two-step procedure can reach around 50%.[3,6]

Recently, we reported a new single-step (SS) synthesis for InP/ZnS NCs showing even higher QY (60−70%).[5] In this method, both the core (In, P) and the shell (Zn, S) precursors were mixed at room temperature and then quickly heated to 250−300 °C. We proposed that the InP core NCs started to form at low temperature (60−80 °C), followed by deposition of the ZnS shell at higher temperature (230−300 °C) due to the difference in reactivity of the InP and ZnS precursors. However, ion exchange is an important phenomenon occurring at the high temperatures used for both TS and SS synthesis of few nanometer InP/ZnS NCs, which could lead to an interfacial alloy layer between core and shell especially for the two similar anions P and S. In turn, an alloyed or graded internal structure of NCs can have a very important influence on their electronic and optical properties. A good example is the blinking suppression observed in alloyed core/shell CdZnSe/ZnSe NCs in contrast to conventional core/shell CdSe/ZnSe NCs exhibiting the typical blinking behavior.[8] The authors suggested that the non-blinking properties of their CdZnSe/ZnSe NCs could be attributed to their radially graded alloy structure. However, without clear evidence of the internal structure of the NCs, the physical processes influencing the emission of light in relation with the NC structure cannot be unraveled, thus making it difficult to further optimize NCs'

*Address correspondence to olivier.renault@cea.fr, peter.reiss@cea.fr.

Received for review March 22, 2010 and accepted July 19, 2010.

Published online July 28, 2010.
10.1021/nn100581t

performances through controlled changes of the synthesis conditions. A detailed understanding of the internal structure of luminescent semiconductor NCs, going beyond the simple discrimination between a core/shell and a homogeneous structure and giving access to the core/shell interface properties, is lacking to date.

The general scheme for the investigation of the NCs' properties is the combination of optical (*e.g.*, UV−vis, PL) and structural (*e.g.*, XRD, TEM) analyses. Due to the intrinsically small diameter of the NCs and the low lattice mismatch between core and shell materials, TEM techniques are very difficult to implement with the purpose to probe the internal structure. Spectroscopic investigations using the STEM-EELS or STEM-EDS modes have been successfully used to put into evidence core/shell structures but fail to provide clear information in the case of graded structures.[8] Photoemission techniques have been used more advantageously by several groups to derive the composition information on heterostructure core/shell NCs. For instance, X-ray photoelectron spectroscopy (XPS) studies were reported on CdSe/ZnSe,[9] CdSe/ZnS,[10] and InP/ZnS[7] core/shell NCs as well as for InAs NCs with various shell materials (InP, GaAs, CdSe, ZnSe, ZnS).[11] In these examples, the appearance of the XPS signals of the shell material was used to confirm the existence of core/shell structure. Other authors evidenced the presence of spherical core/shell NCs and characterized the shell density by means of angle-resolved XPS[12] or studied quantitatively the oxidation kinetics of NCs with fixed-angle XPS.[13] However, since a conventional X-ray source (Al Kα or Mg Kα) was used in these experiments, the core/shell interface properties could not be examined due to the relatively low energy resolution. More importantly, in-depth studies are not possible with laboratory-based XPS instrumentation, in which the only parameter that changes the escape depth is the photoelectron takeoff angle which remains constant in the case of the typical spherical geometry of NCs. In contrast to these XPS studies using an X-ray source of fixed energy, the improved brilliance, high-energy resolution, energy tunability, and surface sensitivity down to a few angstroms make soft X-ray photoelectron spectroscopy (SXPS) with synchrotron radiation an attractive tool to characterize core/shell NCs with accurate in-depth resolution. In this case, the escape depth can be varied easily by tuning the photon energy.

Borchert *et al.* first applied this technique to the InP/ZnS system.[14] Several other studies report the use of SXPS to investigate CdSe/ZnS,[15] CdS/HgS/CdS,[16] and InAs/CdSe core/shell NCs.[17] In the original work of Borchert *et al.*, the InP core attenuation by the ZnS shell was deduced from the increase of the core-to-shell (InP-to-ZnS) intensity ratio with increasing photoelectron kinetic energy, equivalent to an increase of the escape depth as the photon energy increases. However, in all of the above cited works, it was not possible to probe precisely enough the internal core/shell structure of the NCs because the energy resolution used (∼300 meV in the best case) did not allow distinguishing subtle differences in the chemical environment within the heterostructure. Therefore, probing the internal heterostructure and the core/shell interface in sub-10 nm NCs still remains a big challenge.

In this article, we present the results of a detailed in-depth study of InP/ZnS NCs using high-energy resolution SXPS of the In3*d* core level, which enables us to unravel their internal structure in a way not previously demonstrated at such a level of accuracy. The performed compositional analysis benefited from the high instrumental resolution reaching 122 meV. We investigated two different types of NCs synthesized using the conventional two-step or the above-mentioned single-step methods and named as InP/ZnS-TS and InP/ZnS-SS, respectively. Our study gives insight into the formation process of these two systems and allows correlation between their internal structures and optical properties.

RESULTS AND DISCUSSION

For the chemical state analysis of the internal structure of the NCs, the In3*d* core level was considered because In is the metal element of the NCs' core; compared to Zn, the main photoelectric transition has a much lower binding energy (In3$d_{5/2}$ ∼ 445 eV, Zn2$p_{3/2}$ ∼ 1022 eV), with a much higher photoionization cross section. Combined with some instrumental issues inherent to the beamline during the experiment, which was delivering much lower flux at high photon energy (due to carbon contamination of the optics) at considerably less overall energy resolution, all of this was making the acquisition of meaningful, high-resolution Zn2*p* signals more difficult and of considerably less interest for our purpose. For the acquisition of In3$d_{5/2}$, the photon energy was set successively at $h\nu = 546$, 746, and 986 eV, which yielded increasing escape depth of the In3$d_{5/2}$ photoelectrons due to the increasing kinetic energy of 100, 300, and 540 eV, respectively. In this way, the sensitivity of the analysis could be tuned from the shell (lower In3$d_{5/2}$ kinetic energies) down to the core/shell interface (higher In3$d_{5/2}$ kinetic energies). The novelty of the present measurements is the very high energy resolution employed, which is crucial for discriminating in a reliable way fine changes of the In chemical state that could be due to a chemically non-abrupt core/shell interface and the existence of an intermediate shell. The spectral width of the synchrotron soft X-ray beam was 40−200 meV in the explored energy range; combined with an analyzer broadening of 110 meV or less in the conditions used, the overall energy resolution of the analysis was therefore less than 225 meV. More precisely, the energy resolution was respectively 122, 186, and 225 meV at 546, 746, and 986 eV photon energies, respectively. The C1*s* peak was used as a reference for the binding energy scale (284.6 eV).

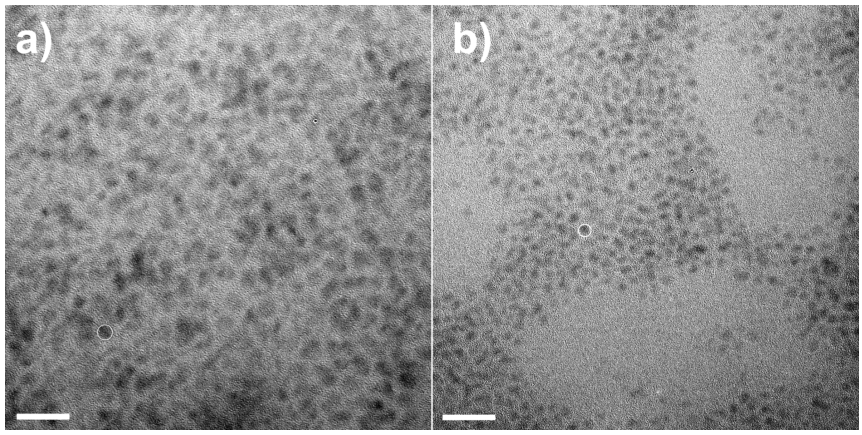

Figure 1. TEM image of the InP/ZnS-TS (a) and InP/ZnS-SS (b) NCs. The scale bar corresponds to 20 nm. In each case, one NC is highlighted to indicate the diameter.

Figure 1 shows representative TEM images of InP/ZnS-TS and InP/ZnS-SS NCs, illustrating both the size and uniformity of the NCs. The diameters of the InP/ZnS-TS and InP/ZnS-SS NCs have been determined as 5.1 and 3.6 nm, respectively. It has to be pointed out that—although larger particles would facilitate our study—the size of NCs obtained with the single-step method is limited to 3−4 nm. On the one hand, adding the shell precursors right from the beginning blocks the core NCs' growth at early stages of the reaction. The thickness of the ZnS shell, on the other hand, rapidly reaches a plateau due to the relatively low reactivity of the applied precursors, zinc stearate and dodecanethiol.[5]

The In3$d_{5/2}$ spectra of the two samples are shown in Figure 2 and Figure 3. The first striking qualitative result is the evolution of the core level intensity profile with photon energy that appears to be very different for the InP/ZnS-TS and InP/ZnS-SS NCs: in the case of the InP/ZnS-TS NCs, the In3$d_{5/2}$ line shape varies continuously as the photon energy (or the In3$d_{5/2}$ photoelectron escape depth) increases, whereas for the InP/ZnS-SS NCs, the line shape remains almost unchanged. This is already a strong indication that the In-related chemical states are not localized the same way deep inside the SS- and TS-NCs. In order to go into more quantitative details, we considered the fitting of the experimental intensity profiles. The results are displayed in Figures 2 and 3, while the details of the fitting procedure are supplied in the Supporting Information. The high-resolution core level In3$d_{5/2}$ spectra of both InP/ZnS-TS (Figure 2) and InP/ZnS-SS (Figure 3) were fitted in the same manner with three chemical state components of similar binding energies (444.4, 445.0, and 445.7 eV). What is first worth noting is that the relative intensities of the three components behave not the same way as a function of photon energy between InP/ZnS-TS and InP/ZnS-SS, which confirms our previous assumption regarding a different in-depth distribution of the In-related chemical states: for the InP/ZnS-TS spectra, we see a strong evolution of the relative intensities with photon energy. For the InP/ZnS-SS NCs, almost no change is observed.

We now address the issue of the assignment of the three In3$d_{5/2}$ chemical state components. The component at 444.4 eV is assigned to In−P, which is consistent with the reported value of bulk In−P (444.5 eV).[18] The components at 445.0 and 445.7 eV would normally be considered as InPO and $InPO_3$ contributions, respectively, in the case of oxidation of the InP NCs. However, oxidation is unlikely in the synthesis process used here, which took place entirely under inert atmosphere without intermediate purification of the core NCs before the shell growth. No indium oxide was observed in the powder X-ray diffractogram, which therefore rules out

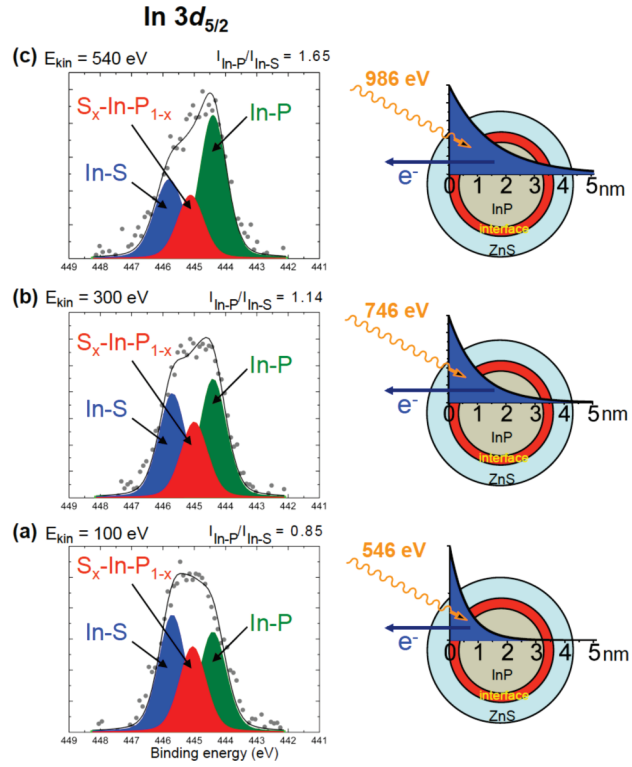

Figure 2. Left: High-resolution core level In3$d_{5/2}$ spectra of InP/ZnS-TS NCs at three kinetic energies of (a) 100, (b) 300, and (c) 540 eV corresponding to three photon energies of 546, 746, and 986 eV, respectively. The experimental intensity is represented by the gray solid dots, while the fitted profile is shown as the black line. Right: Schematic of the InP/ZnS-TS NCs' internal structure derived from the high-resolution core level spectra; the attenuation with depth of the photoemitted In3*d* signal, plotted for the calculated values of the inelastic mean free path (0.6, 1.0, 1.5 nm at 100, 300, 540 eV kinetic energy, respectively), is superimposed to visualize the change of the relative contributions to the signal of the interface and the core as a function of kinetic energy.

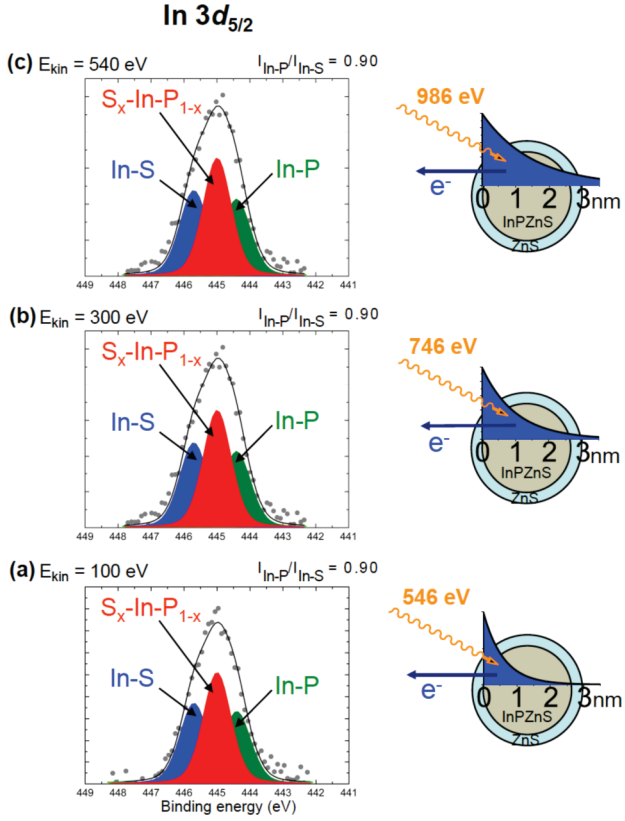

Figure 3. Left: High-resolution core level In3$d_{5/2}$ spectra of InP/ZnS-SS NCs at three kinetic energies of (a) 100, (b) 300, and (c) 540 eV corresponding to three photon energies of 546, 746, and 986 eV, respectively. The experimental intensity is represented by the gray solid dots, while the fitted profile is shown as the black line. Right: Scheme of the InP/ZnS-SS NCs' internal structure derived from the high-resolution spectra, together with the attenuation with depth of the photoemitted In3*d* signal, plotted for the calculated values of the inelastic mean free path (0.6, 1.0, 1.5 nm for 100, 300, 540 eV kinetic energy, respectively).

any oxidation event.[4] Therefore, the components at 445.7 and 445.0 eV were attributed to In−S and S_x−In−P_{1-x}, respectively. The In−S component at 445.7 eV is consistent with the reported value of 445.5 eV.[19] In summary, for InP/ZnS-TS NCs, we observe three chemical state components assigned to In−P, In−S, and S_x−In−P_{1-x}. This interpretation is also supported qualitatively by the observed intensities as a function of photon energy expected for a InP/ZnS core−shell structure: the In−P-related component is more intense in bulk-sensitive conditions ($h\nu$ = 986 eV) but much weaker relative to the others in surface-sensitive conditions ($h\nu$ = 546 eV); an opposite behavior is observed for the more surface-related In−S and S_x−In−P_{1-x} components. The quantitative analysis presented further below confirms this. From this first result, we then evidence an interface shell with mixed In−S and S_x−In−P_{1-x} chemical states between the InP core and the ZnS shell. The In−S and S_x−In−P_{1-x} states are thought to be formed *via* S and P anion exchange. Ion exchange generally plays an important role in nanomaterials, such as nanowires,[20−23] nanorods,[24] and nanocrystals.[25−27] Indeed, S and P ion exchange has been reported to take place even at low temperature (~60 °C) for a sulfur-passivated surface of bulk InP in the presence of a $(NH_4)_2S$ solution or H_2S gas.[18,19,28−31]

In the two-step procedure used here, interdiffusion of the S and P anions is favored by the high reaction temperature, which can lead to the complete exchange of the In−P surface with In−S and formation of an underlying S_x−In−P_{1-x} layer. In contrast to these findings, in ref 14, the interface between InP and ZnS was assumed to be sharp without any interfacial layer, although, similar to our method, the core/shell structure was synthesized in a two-step procedure at high temperature (over 200 °C). As discussed above, ion exchange is very likely to occur at such high temperatures. Therefore, an alloyed interface layer composed of In−P, S_x−In−P_{1-x}, and In−S components between the InP core and the ZnS shell is a more suitable description.

We now assess the relative intensities and changes of In-related chemical states with depth, as observed in the spectra of Figures 2 and 3, taking into account the photoelectron inelastic mean free path λ_{In} of the In3$d_{5/2}$ photoelectrons. The collected In3$d_{5/2}$ signal originates from In atoms within the NCs. The attenuation of each component depends on the distance of the photoemitting atom from the surface. By definition, after a traveling distance to the surface of λ_{In}, the signal is attenuated by a factor 1/*e*, and therefore, λ_{In} is usually referred to as the escape depth. The organic ligand shell covering the surface of the NCs is expected to attenuate the In3*d* signal; however, it will not change the line shape of the spectra in Figures 2 and 3. Furthermore, on the basis of previous reports, the surface coverage of the organic layer is estimated to not be higher than 50%: in the case of CdSe NCs,[33] the coverage was determined to be diameter-dependent, varying from 60% in 1.8 nm NCs down to 30% in 6 nm NCs; in the case of 5.6 nm InP/ZnS NCs, the surface coverage with organic ligands has been estimated to lie in the range of 25−50%.[14] Therefore, the detection of the topmost surface-sensitive signal, emitted by In atoms located below the fraction of the NC surface not covered by ligands, is possible. The inelastic mean free path λ_{In} is strongly dependent on the photoelectron kinetic energy, which enables the observation of highly depth-resolved chemical changes.

We calculated λ_{In} using the TPP-2 M formula based on bulk densities for InP (4.81 g/cm^3) and ZnS (3.98 g/cm^3) and band gaps of InP NCs in the quantum confinement regime (1.75 eV for the TS sample, 2.38 eV for the SS sample) and of bulk ZnS (3.6 eV).[32] Value of λ_{In} is found to be identical in InP and ZnS; therefore, both TS and SS-NCs behave as a uniform medium considering the attenuation of the In3*d* signal, irrespective to their internal structure. The calculated values for λ_{In} are 0.6, 1.0, and 1.5 nm at the three kinetic energies of 100, 300, and 540 eV; λ_{In} is therefore lower than the

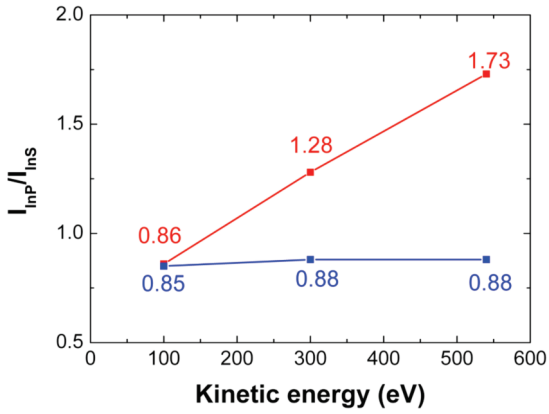

Figure 4. Average intensity ratio of In−P to In−S components for InP/ZnS-TS (red) and InP/ZnS-SS (blue) at three photon energies. The values account for variable fitting conditions regarding the S_x−In−P_{1-x}/In−S intensity ratio, which essentially leaves the evolution of In−P/In−S as a function of kinetic energy unaffected in both cases. In the case of InP/ZnS-TS NCs, the In−P/In−S ratio increases from 0.86 over 1.28 to 1.73 with increasing kinetic energy, whereas it remains nearly constant in the case of InP/ZnS-SS NCs.

NCs radius, which is 1.8 nm for InP/ZnS-SS and 2.55 nm for InP/ZnS-TS NCs. From the calculated values, we represented for each kinetic energy the exponential signal attenuation of the In3*d* signal with depth (right panels of Figures 2 and 3). The origin of the depth scale corresponds to the In atoms closest to the NC surface in each case. Considering first Figure 2, the important point is that strong changes in the In3$d_{5/2}$ profile shape, corresponding to changes in chemical composition, can now be related to different depths from the In atomic layers in the TS NCs particles (In−S chemical states at the interface between the InP core and the ZnS shell). By decreasing the kinetic energy, we clearly see that the variations in relative intensity of the components correspond to the increasing weight of the interface component. In the case of InP/ZnS-SS NCs (Figure 3), the spectral weight of the chemical states arising from the outermost In atoms probed at 100 eV kinetic energy is very different from that of the InP/ZnS-TS NCs. Furthermore, the In−P/In−S ratio remains constant when the depth increases by a value corresponding to the mean free path. This is clear evidence of the different internal structure of the two types of NCs.

Figure 4 represents the summary of the evolution with probing depth observed for the In−P and In−S chemical state intensity ratios. Each point is the average of 10 fitting results (see Supporting Information). At the lowest kinetic energy of 100 eV, In3$d_{5/2}$ photoelectrons escape mainly from the interface layer between the InP core and the ZnS shell, and an intensity ratio of In−P to In−S of 0.86 is found. The ratio increases steadily up to 1.73 with kinetic energy, which further confirms that the in-depth distribution of indium chemical states is not uniform. It is therefore reasonable to assume that the alloyed interface layer is not homogeneous, but shows a higher fraction of the In−S component closer to the ZnS shell and a lower one close to the InP core. One can explain this behavior by considering that P−S ion exchange takes place preferentially at the InP NC surface and is limited by the quantity of the initially injected S precursor. This assumption is supported by a recently reported synchrotron radiation XPS analysis of ZnS/CdSe/ZnS core/shell/shell NCs, which exhibit a compositional gradient close to the inner ZnS/CdSe interface and a sharp compositional change between CdSe and the outer ZnS shell.[34] In summary, our results are consistent with InP/ZnS-TS NCs having a core/interface layer/shell structure composed of a pure InP core, a graded alloyed S_x−In−P_{1-x} interface layer, and a relatively pure ZnS shell, respectively.

Let us now compare quantitatively the results of the InP/ZnS-SS NCs with those of the InP/ZnS-TS NCs. Upon increase of photon energy, the In3$d_{5/2}$ spectra do not exhibit any change of the component relative intensities, and the spectra are always dominated by a large S_x−In−P_{1-x} component at 445.0 eV. The calculated intensity ratio of In−P/In−S shown in Figure 3 remains at a constant value of 0.90, and the relative intensity of the S_x−In−P_{1-x} component does not change when increasing photon energy. It can therefore be concluded that InP/ZnS-SS has a homogeneous alloyed InPZnS core containing In−P, S_x−In−P_{1-x}, and In−S components in a fixed ratio. The one-step synthesis process of InP/ZnS-SS NCs favors interdiffusion due to the sulfur and zinc precursors being present already in the beginning of the synthesis. The presence of zinc ions, required for charge neutrality, resulted in a strong increase of the S_x−In−P_{1-x} component as compared to In−S and In−P and to the situation in the InP/ZnS-TS structure. The evolution of the elemental composition of the NCs with reaction time, determined by EDX analysis,[5] shows that the S content with respect to P is approximately 1:1 in the beginning of reaction (from 5 to 10 min), which supports the hypothesis of the formation of homogeneous alloyed InPZnS NCs. The In content reached its maximum at 30 min, while the Zn and S contents continuously increased until 60 min, indicating ZnS shell formation after complete depletion of the In precursor.[5] Thus, the InP/ZnS-SS NCs are composed of a homogeneous alloyed InPZnS core capped with a (thin) shell of pure ZnS. Accordingly, with an escape depth increasing from 0.6 to 1.5 nm, the same proportion of In3$d_{5/2}$ photoelectrons was detected from the core due to its homogeneous alloyed structure.

The quantitative analysis of the relative intensities performed so far, as a function of photon energy, support the model of two distinct in-depth distributions: first, a heterogeneous one with the InP core and an alloyed In−S/S_x−In−P_{1-x} core−shell interface (InP/ZnS-TS NCs); second, a homogeneous one reflecting an alloyed chemical structure (InP/ZnS-SS NCs). We also evidence a chemical state component assigned to mixed S and P bonding of In within the NCs, located at the core−shell interface for InP/ZnS-TS NCs. To the best

of our knowledge, this observation of the S_x-In-P_{1-x} component in the In3$d_{5/2}$ signal reported for the first time here benefited from the high-energy resolution of the SXPS analysis. Although the S_x-In-P_{1-x} component has been suggested previously in several publications,[28,29,31] no spectral evidence related to this component has been reported so far. Equally, the core level spectrum of In3*d* was considered in ref 14; however, the detailed compositional analysis based on In3*d* has not been performed due to a much lower instrumental resolution. For InAs/CdSe NCs,[17] two components due to the photoemission from volume (In−As) and interfacial (In−Se) In atoms were observed in the In3$d_{5/2}$ spectrum. These signals have been attributed to a "Se-rich" interface layer; however, a possible $As_x-In-Se_{1-x}$ component was not suggested by the authors.

The observation of the In−S and S_x-In-P_{1-x} components enables a better understanding of both the reaction mechanism and of the optical properties of InP/ZnS NCs. In the case of the two-step synthesis procedure of InP/ZnS-TS,[4] pure InP core NCs were synthesized by reacting indium myristate with PH_3 gas at 250 °C for 30 min. The fluorescence QY of these NCs is very low, on the order of 1%. With the addition of a small quantity of zinc stearate and zinc ethylxanthate at 300 °C, the reaction attained a surface alloying stage by P and S anion exchange and formation of the interface layer comprising the In−P, S_x-In-P_{1-x}, and In−S components. The QY reaches values of 8−10% during this stage, possibly due to the passivation of surface trap states. During the addition of the second portion of zinc stearate and zinc ethylxanthate at 210 °C to form the pure ZnS shell, the QY increases to values of 15−40% depending on the core NCs' size.

Figure 5 shows the UV−vis and PL spectra of the final InP/ZnS-TS NCs used in this study, which exhibit the excitonic peak at 660 nm and the PL peak at 710 nm. For the one-pot synthesis procedure of InP/ZnS-SS NCs, a continuous red shift of the UV−vis and PL spectra with reaction time has been observed.[5] This behavior already indicated the formation of an alloyed rather than a core/shell structure; as for the latter, the emission wavelength should be blocked after ZnS shell formation. The InP/ZnS-SS NC sample used here shows the excitonic peak at 460 nm and the PL peak at 520 nm (Figure 5).

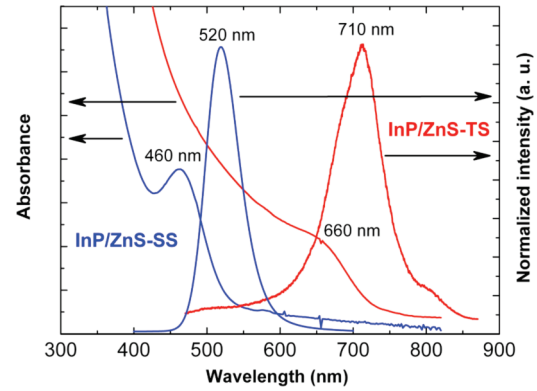

Figure 5. UV−vis absorption and PL spectra of InP/ZnS-TS (red, excitation wavelength = 450 nm) and InP/ZnS-SS (blue, excitation wavelength = 370 nm) NCs.

CONCLUSIONS

We have shown that high- resolution XPS core level analysis using tunable energy soft X-ray synchrotron radiation is a powerful tool to precisely probe the internal structure of small heterostructure NCs. The high-energy resolution below 200 meV enabled the identification of a previously only postulated S_x-In-P_{1-x} component. It exists in InP/ZnS core/shell NCs prepared in a two-step procedure as a graded interface layer between the InP core and ZnS shell. Our study further revealed that InP/ZnS NCs prepared with a single-step method consist of a homogeneous InPZnS alloy structure with a thin ZnS shell. The clear spectroscopic evidence of the different In chemical states helps to identify the involved reaction mechanisms and to understand the (photo)physical properties of the NCs. It can be expected that the use of this technique will be extended to other types of heterostructures at the nanoscale presenting low *Z*-contrast, for which the applicability of high-resolution TEM techniques is reaching its limits.

MATERIALS AND METHODS

InP/ZnS-TS NCs were synthesized using a two-step procedure reported earlier:[4] (i) the indium precursor (indium myristate in 1-octadecene) was reacted with *in situ* generated PH_3 gas at 250 °C for 30 min to form the core InP NCs; (ii) one part of a mixture of zinc stearate and zinc ethylxanthate (3:1) in 1-octadecene was added into a InP NC dispersion and heated to 300 °C to form a thin InP/ZnS interfacial layer before injecting slowly the second part of this mixture at 210 °C to increase the shell thickness. The InP/ZnS-SS NCs were synthesized in a single-step procedure,[5] which consists of mixing all precursors (indium myristate, zinc stearate, tris(trimethylsilyl)phosphine, and dodecanethiol) in a 1:1:1:1 ratio in 1-octadecene at room temperature and subsequently heating to 270−300 °C for a certain time (5 min to 2 h). To perform the SXPS experiments, a drop of a diluted dispersion of the NCs in toluene was deposited on a natively oxidized silicon substrate. The sample was then rinsed with *n*-hexane, dried under vacuum, and placed in the XPS analysis chamber. This procedure provided a monolayer of NCs on the SiO_2 surface and prevented from charging during the SXPS experiments.

High-resolution core level X-ray photoelectron spectroscopy with synchrotron radiation was carried out at the third generation SOLEIL storage ring operated in the top-up mode at 300 mA, using the photoemission endstation of the TEMPO beamline, which covers an energy range of 50−1500 eV. The experiments were performed at room temperature and at a base pressure of 2×10^{-10} mbar. Photoelectrons were analyzed at a takeoff angle of 90° with respect to the sample surface using a Scienta SES 2002 hemispherical analyzer and delay-line detector.

Acknowledgment. Financial support from the European Commission under the sixth Framework Programme (FP6) Thematic Priority: Nanotechnologies and nanosciences, knowledge-based multifunctional materials and new production processes and devices (NMP) (Project "Hybrid Ultra Precision Manufacturing Process Based on Positional- and Self-assembly for Complex Micro-Products, HYDROMEL"), from the French Research Agency ANR (Project PNANO "SYNERGIE"), and from CEA (program Technologies pour la Santé, Project "TIMOMA2") is acknowledged.

Supporting Information Available: Details of the fitting process: fitting results, residual spectra, and used fitting parameters. This material is available free of charge *via* the Internet at http://pubs.acs.org.

REFERENCES AND NOTES

1. Reiss, P.; Protière, M.; Li, L. Core/Shell Semiconductor Nanocrystals. *Small* **2009**, *5*, 154–168.
2. Haubold, S.; Haase, M.; Kornowski, A.; Weller, H. Strongly Luminescent InP/ZnS Core−Shell Nanoparticles. *ChemPhysChem* **2001**, *2*, 331–334.
3. Xie, R.; Battaglia, D.; Peng, X. Colloidal InP Nanocrystals as Efficient Emitters Covering Blue to Near-Infrared. *J. Am. Chem. Soc.* **2007**, *129*, 15432–15433.
4. Li, L.; Protière, M.; Reiss, P. Economic Synthesis of High Quality InP Nanocrystals Using Calcium Phosphide as the Phosphorus Precursor. *Chem. Mater.* **2008**, *20*, 2621–2623.
5. Li, L.; Reiss, P. One-Pot Synthesis of Highly Luminescent InP/ZnS Nanocrystals without Precursor Injection. *J. Am. Chem. Soc.* **2008**, *130*, 11588–11589.
6. Xu, S.; Ziegler, J.; Nann, T. Rapid Synthesis of Highly Luminescent InP and InP/ZnS Nanocrystals. *J. Mater. Chem.* **2008**, *18*, 2653–2656.
7. Ryu, E.; Kim, S.; Jang, E.; Jun, S.; Jang, H.; Kim, B.; Kim, S.-W. Step-Wise Synthesis of InP/ZnS Core−Shell Quantum Dots and the Role of Zinc Acetate. *Chem. Mater.* **2009**, *21*, 573–575.
8. Wang, X.; Ren, X.; Kahen, K.; Hahn, M. A.; Rajeswaran, M.; Maccagnano-Zacher, S.; Silcox, J.; Cragg, G. E.; Efros, A. L.; Krauss, T. D. Non-blinking Semiconductor Nanocrystals. *Nature* **2009**, *459*, 686–689.
9. Hoener, C. F.; Allan, K. A.; Bard, A. J.; Campion, A.; Fox, M. A.; Mallouk, T. E.; Webber, S. E.; White, J. M. Demonstration of a Shell−Core Structure in Layered Cadmium Selenide−Zinc Selenide Small Particles by X-ray Photoelectron and Auger Spectroscopies. *J. Phys. Chem.* **1992**, *96*, 3812–3817.
10. Dabbousi, B. O.; Rodriguez-Viejo, J.; Mikulec, F. V.; Heine, J. R.; Mattoussi, H.; Ober, R.; Jensen, K. F.; Bawendi, M. G. (CdSe)ZnS Core−Shell Quantum Dots: Synthesis and Characterization of a Size Series of Highly Luminescent Nanocrystallites. *J. Phys. Chem. B* **1997**, *101*, 9463–9475.
11. Cao, Y.; Banin, U. Growth and Properties of Semiconductor Core/Shell Nanocrystals with InAs Cores. *J. Am. Chem. Soc.* **2000**, *122*, 9692–9702.
12. Tunc, I.; Suzer, S.; Correa-Duarte, M. A.; Liz-Marzán, L. M. XPS Characterization of Au (Core)/SiO_2 (Shell) Nanoparticles. *J. Phys. Chem. B* **2005**, *109*, 7597–7600.
13. Yang, D.-Q.; Gillet, J.-N.; Meunier, M.; Sacher, E. Room Temperature Oxidation Kinetics of Si Nanoparticles in Air, Determined by X-ray Photoelectron Spectroscopy. *J. Appl. Phys.* **2005**, *97*, 024303.
14. Borchert, H.; Haubold, S.; Haase, M.; Weller, H.; McGinley, C.; Riedler, M.; Möller, T. Investigation of ZnS Passivated InP Nanocrystals by XPS. *Nano Lett.* **2002**, *2*, 151–154.
15. Borchert, H.; Talapin, D. V.; McGinley, C.; Adam, S.; Lobo, A.; de Castro, A. R. B.; Möller, T.; Weller, H. High Resolution Photoemission Study of CdSe and CdSe/ZnS Core−Shell Nanocrystals. *J. Chem. Phys.* **2003**, *119*, 1800–1807.
16. Borchert, H.; Dorfs, D.; McGinley, C.; Adam, S.; Möller, T.; Weller, H.; Eychmüller, A. Photoemission Study of Onion Like Quantum Dot Quantum Well and Double Quantum Well Nanocrystals of CdS and HgS. *J. Phys. Chem. B* **2003**, *107*, 7486–7491.
17. McGinley, C.; Borchert, H.; Talapin, D. V.; Adam, S.; Lobo, A.; de Castro, A. R. B.; Haase, M.; Weller, H.; Möller, T. Core-Level Photoemission Study of the InAs/CdSe Nanocrystalline System. *Phys. Rev. B* **2004**, *69*, 045301.
18. Tao, Y.; Yelon, A.; Sacher, E.; Lu, Z. H.; Graham, M. J. S-Passivated InP (100) (1 × 1) Surface Prepared by a Wet Chemical Process. *Appl. Phys. Lett.* **1992**, *60*, 2669–2671.
19. Fukuda, Y.; Suzuki, Y.; Sanada, N.; Sasaki, S.; Ohsawa, T. $(NH_4)_2S_x$-Treated InP(001) Studied by High-Resolution X-ray Photoelectron Spectroscopy. *J. Appl. Phys.* **1994**, *76*, 3059–3062.
20. Jeong, U.; Xia, Y.; Yin, Y. Large-Scale Synthesis of Single-Crystal CdSe Nanowires through a Cation-Exchange Route. *Chem. Phys. Lett.* **2005**, *416*, 246–250.
21. Jeong, U.; Camargo, P. H. C.; Lee, Y. H.; Xia, Y. Chemical Transformation: A Powerful Route to Metal Chalcogenide Nanowires. *J. Mater. Chem.* **2006**, *16*, 3893–3897.
22. Schoen, D. T.; Peng, H.; Cui, Y. Anisotropy of Chemical Transformation from In_2Se_3 to $CuInSe_2$ Nanowires through Solid State Reaction. *J. Am. Chem. Soc.* **2009**, *131*, 7973–7975.
23. Dloczik, L.; Engelhardt, R.; Ernst, K.; Fiechter, S.; Sieber, I.; Konenkamp, R. Hexagonal Nanotubes of ZnS by Chemical Conversion of Monocrystalline ZnO Columns. *Appl. Phys. Lett.* **2001**, *78*, 3687–3689.
24. Sadtler, B.; Demchenko, D. O.; Zheng, H.; Hughes, S. M.; Merkle, M. G.; Dahmen, U.; Wang, L.-W.; Alivisatos, A. P. Selective Facet Reactivity during Cation Exchange in Cadmium Sulfide Nanorods. *J. Am. Chem. Soc.* **2009**, *131*, 5285–5293.
25. Son, D. H.; Hughes, S. M.; Yin, Y.; Alivisatos, A. P. Cation Exchange Reactions in Ionic Nanocrystals. *Science* **2004**, *306*, 1009–1012.
26. Camargo, P. H. C.; Lee, Y. H.; Jeong, U.; Zou, Z.; Xia, Y. Cation Exchange: A Simple and Versatile Route to Inorganic Colloidal Spheres with the Same Size but Different Compositions and Properties. *Langmuir* **2007**, *23*, 2985–2992.
27. Zhong, X.; Han, M.; Dong, Z.; White, T. J.; Knoll, W. Composition-Tunable $Zn_xCd_{1-x}Se$ Nanocrystals with High Luminescence and Stability. *J. Am. Chem. Soc.* **2003**, *125*, 8589–8594.
28. Gallet, D.; Hollinger, G. Chemical, Structural, and Electronic Properties of Sulfur-Passivated InP(001) (2 × 1) Surfaces Treated with $(NH_4)_2S_x$. *Appl. Phys. Lett.* **1993**, *62*, 982–984.
29. Chasse, T.; Chasse, A.; Peisert, H.; Streubel, P. Sulfur-Modified Surface of InP(001): Evidence for Sulfur Incorporation and Surface Oxidation. *Appl. Phys. A: Mater. Sci. Process.* **1997**, *65*, 543–549.
30. Gebhardt, R. K.; Preobrajenski, A. B.; Chasse, T. Core and Valence-Level Photoemission Study of the InP(001)-(2 × 1)S Surface: Surface Structure and Electronic States. *Phys. Rev. B* **2000**, *61*, 9997–10000.
31. Hung, W.-H.; Chen, H.-C.; Chang, C.-C.; Hsieh, J.-T.; Hwang, H.-L. Adsorption and Decomposition of H_2S on InP(100). *J. Phys. Chem. B* **1999**, *103*, 3663–3668.
32. Tanuma, S.; Powell, C. J.; Penn, D. R. Calculations of Electron Inelastic Mean Free Paths. III. Data for 15 Inorganic Compounds over the 50−2000 eV Range. *Surf. Interface Anal.* **1991**, *17*, 927–939.
33. Katari, J. E. B.; Colvin, V. L.; Alivisatos, A. P. X-ray Photoelectron Spectroscopy of CdSe Nanocrystals with Applications to Studies of the Nanocrystal Surface. *J. Phys. Chem.* **1994**, *98*, 4109–4117.
34. Santra, P. K.; Viswanatha, R.; Daniels, S. M.; Pickett, N. L.; Smith, J. M.; O'Brien, P.; Sarma, D. D. Investigation of the Internal Heterostructure of Highly Luminescent Quantum Dot−Quantum Well Nanocrystals. *J. Am. Chem. Soc.* **2009**, *131*, 470–477.